This is a repository copy of *An inverse method for optimizing elastic properties considering multiple loading conditions and displacement criteria*.

White Rose Research Online URL for this paper:
http://eprints.whiterose.ac.uk/146264/

Version: Accepted Version

An inverse method for optimizing elastic properties considering multiple loading conditions and displacement criteria

Danny Smyl
Department of Mechanical Engineering
Aalto University
Espoo, Finland 02150
Email: danny.smyl@aalto.fi

Significant research effort has been devoted to topology optimization of two- and three-dimensional structural elements subject to various design and loading criteria. While the field of topology optimization has been tremendously successful over the years, literature focusing on the optimization of spatially-varying elastic material properties in structures subject to multiple loading states is scarce. In this article, we contribute to the state of the art in material optimization by proposing a numerical regime for optimizing the distribution of the elastic modulus in structural elements subject to multiple loading conditions and design displacement criteria. Such displacement criteria (target displacement fields prescribed by the designer) may result from factors related to structural codes, occupant comfort, proximity of adjacent structures, etc. In this work, we utilize an inverse problem based framework for optimizing the elastic modulus distribution considering N target displacements and imposed forces. This approach is formulated in a straight-forward manner such that it may be applied in a broad suite of design problems with unique geometries, loading conditions, and displacement criteria. To test the approach, a suite of optimization problems are solved to demonstrate solutions considering N = 2 for different geometries and boundary conditions.

1 Introduction

Determination of optimal structural geometries, shapes, connectivity, cross-sectional area, and void locations are central themes in topology optimization. In cases where additional degrees of freedom for structural optimization are desirable, one may additionally consider the optimization of macroscopic material properties (such as elastic properties), which is the central theme of this article. With this said, the ability to optimize structural topology – alone – affords designers substantial freedom by reducing structural weight, increasing adherence to architectural constraints, and providing an additional means to meet numerous other design criteria [1–3]. Significant research has been devoted to topology optimization over the last thirty years, often aiming to optimize geometrical aspects of structural elements (voids, connectivity, thickness, etc.). In this effort, various topology optimization approaches including the well-known "solid isotropic material with penalization" (SIMP) regime [4–6], level-set methods [7–11], phase-field methods [12–14], and other emerging regimes have had much success.

Complimenting topology optimization is the optimization of elastic material properties (herein referred to as simply *material optimization*), wherein the distribution of elastic material properties is optimized with respect to the design criteria [15]. Material optimization may be broadly viewed as a part of "free material design" (FMD), which often aims to maximize structural stiffness by optimizing the material and material distribution given some design criteria and constraints [16]. Classically, these criterion are incorporated by prescribing the cost of design; generally, the cost Π is is defined by some integral over the domain of interest Ω as follows

$$\Pi = \int_{\Omega} \Phi(\mathbb{C}) dx \qquad (1)$$

where Φ is a scalar function and $\mathbb{C}$ is an elastic tensor in the Cartesian coordinate system x. Arguments incorporated with the scalar cost function $\Phi(\cdot)$ vary upon the design criteria, optimization variables, and prescribed constraints. In cases where only the material thickness, voids, topology, etc. are optimized, the values of the elastic constants are generally distributed equally within Ω.

The attractiveness of material optimization is that it affords designers additional flexibility by increasing the degrees of freedom within Ω – since the models permit inhomogeneity in the elastic parameters. Recently, there has been increased interest in material optimization (e.g. [17–21]); this may, in part, be inspired by emerging engineered materials such as functionally-graded composites, 3D printed materials, fiber-reinforced cement-based composites, and material produced using additive fabrication [15, 22]. One potential advantage of these engineered materials is that their material properties, such as the elastic modulus, may be *inhomogeneous* across the structural geometry. Therefore, the realization of such technologies may promote the usage of material optimization in a large suite of structural applications.

Computational material optimization regimes, often inter-weaved within FMD frameworks, have been well-studied since their origins in seminal works (e.g. [23, 24]), where the authors developed numerical approaches for optimizing materials to achieve minimum compliance. Soon thereafter, researchers utilized regimes employing material and stress constraints (i.e. interior-point methods and penalty-barrier methods), demonstrating improved efficiency in their optimization regimes [25–28]. One aim of constraining the stress during the material optimization process is to prevent structural failure occurring at high stress levels. However, later works showed the difficulties of using stress constraints [29, 30]. The difficulties in utilizing stress constraints often resulted from defining suitable failure criterion and technical complexities in programming stress constraints nested in optimization algorithms [31]. In overcoming these challenges, authors [31–33] developed augmented Lagrangian methods, demonstrating their effectiveness in overcoming obstacles resulting from constraints. Extending the extensive body of work related to constrained materials optimization, researchers in [34, 35] advanced and broadened the state of the art by proposing generic constraints (including displacement and local stress constraints) dependent on design and state variables. Researchers in, e.g. [36–38], have also re-

cently demonstrated the effectiveness of topology optimization regimes incorporating stress constraints coupled with shape sensitivity functions, level-set methods, geometric projection methods, and much more.

Within recent years, substantial research in material optimization has been conducted. Some of the major contributions during this time include publications in isotropic material design (IMD) [39], cubic material design (CMD) [40–42], and Young's modulus design (YMD) [15]. Broadly, the use of these material optimization methods, among the many others mentioned, may be directly applied in conjunction with manufacturing processes utilizing, for example, programming of cellular materials [43], truss-like cellular structures [44,45], cement-based materials [46,47], and functionally-graded materials [48,49]. Moreover, much attention has also been given to optimization problems where the primary focus is not purely related to elasticity. Some examples include the optimization of transport properties in porous materials [50–52], optimization of vessel geometry to promote fluid flow [53–56], and topology optimization for heat conduction problems [57–59].

Although the body of work in material/topology optimization is quite substantial, often many approaches consider only a single load case. In practice, few structural elements experience a unique loading condition through their life cycle. This realization was formally addressed in [16], where the authors proved the existence of a solution to the multi-load optimization problem and a regime for solving the problem with respect to the distribution of the materials as well as the material properties. Since this seminal article, works aiming to optimize structures under multi-load conditions have been noted (e.g. [60–65]). In general, however, literature focusing on the optimization of spatially-varying elastic material properties in structures subject to multiple loading states is scarce.

In this work, we address this gap in research by developing a generic and straight-forward computational framework aiming to determine an optimal distribution of the elastic modulus considering multiple loading conditions and displacement criteria (target displacement fields prescribed by the designer). We reinforce that the aim of the proposed approach is not to optimize the topology or geometry of the structure of interest; rather, we focus solely on the distribution of the elastic modulus. Concisely, in this article we aim to accomplish the following:

1. Develop a straight-forward and generally-applicable inverse problem based framework

for optimizing the elastic modulus distribution considering multiple loading criteria and imposed forces.

2. Determine the effects optimization parameters, the geometry of the structural members, and imposed forces/displacement criteria have on optimized solutions.

3. Analyze the effects that discretization and imposed constraints have on the regime's performance and optimized solutions.

The article is organized as follows. We begin by presenting the mathematical background of the inverse problem and optimization scheme. Following, we demonstrate the approach with numerical examples considering different structural geometries subject to various loading conditions. Thereafter, an analysis of the the effects of discretization and imposed constraints is conducted. Finally, discussion and conclusions are provided.

2 Inverse problem

In this section we propose a regime for optimizing the elastic properties of structural elements using methods rooted in solving inverse problems. We begin by describing inverse problems and how they contrast with classic topology optimization problems. The aim of an inverse problem (for one state) is to find the best parameters ϑ resulting in

$$\mathcal{F}(\vartheta) = d \qquad (2)$$

where $\mathcal{F}$ is a linear or non-linear operator and d is a data set. In the case of a discretized elasticity inverse problem (i) $\mathcal{F}$ is a numerical forward model using, for example the finite element method or finite difference method and (ii) d is a force vector or, most often, displacement field [71]. To solve such a problem, we aim to minimize a functional ψ, with the basic form

$$\psi = ||\mathcal{F}(\vartheta) - d|| \qquad (3)$$

where $||\cdot||$ represents the appropriate norm for the problem (commonly the L_2 or L_1 norm). It is important to recognize that the structure of the inverse problem

is quite different than the structure of a topology optimization functional, which – in a classical sense – aims to minimize the compliance

$$C = U^T K U \qquad (4)$$

where U and K are the displacement field and stiffness matrix for the geometry of interest, respectively. The fundamental objectives of classical topology optimization (TO) and optimization using inverse methods (IM) may now be directly contrasted:

• TO: minimize C given boundary conditions, forces, and design constraints.
• IM: minimize ψ given data set d, operator $\mathcal{F}$, constraints on ϑ, and prior knowledge related to the structure of ϑ.

Some advantages of using inverse methods in elasticity optimization problems are their flexibility to incorporate (a) prior knowledge related to the spatial distribution/structure of ϑ (usually incorporated in regularization techniques), (b) stacked models, i.e. simultaneous solutions for multiple states, and (c) constraints on ϑ, which may result from physically-realistic ranges of a given elastic property or manufacturing limitations. The ability to use (a-c) in determining optimized solutions of elastic properties is the primary motivator for proposing the inverse regime herein.

2.1 Problem Statement

The inverse problem is described as follows: given an unloaded structural geometry Ω, boundary information $\partial\Omega$, N target displacement fields with each state's displacement target concatenated in $\Delta_n = \{\Delta_1, \Delta_2, \Delta_3, \ldots, \Delta_N\}$ (in other words, Δ_n is a stacked vector of displacement fields conforming to any design constraints for structural state n), and loading conditions $F_n = \{F_1, F_2, F_3, \ldots, F_N\}$, find the *inhomogenous* elastic modulus distributions $E_n = \{E_1, E_2, E_3, \ldots, E_N\}$, and simulated displacement fields U_n resulting in

$$\begin{bmatrix} \Delta_1 \\ \Delta_2 \\ \Delta_3 \\ \vdots \\ \Delta_N \end{bmatrix} - \begin{bmatrix} U_1(E_1, F_1) \\ U_2(E_2, F_2) \\ U_3(E_3, F_3) \\ \vdots \\ U_N(E_N, F_N) \end{bmatrix} = \begin{bmatrix} 0 \\ 0 \\ 0 \\ \vdots \\ 0 \end{bmatrix}. \qquad (5)$$

From a more classical viewpoint, we observe that Eq. 5 is equivalent to N systems of concatenated structural equations with each individual state n defined by

$$\Delta_n - U_n = \Delta_n - K_n(E_n)^{-1}F_n = 0 \qquad (6)$$

where K_n is a stiffness matrix determined numerically. The concatenated classical model may then be written in a more classical description using:

$$\begin{bmatrix} \Delta_1 \\ \Delta_2 \\ \Delta_3 \\ \vdots \\ \Delta_N \end{bmatrix} - \begin{bmatrix} K_1(E_1)^{-1}F_1 \\ K_3(E_2)^{-1}F_2 \\ K_3(E_3)^{-1}F_3 \\ \vdots \\ K_N(E_N)^{-1}F_N \end{bmatrix} = \begin{bmatrix} 0 \\ 0 \\ 0 \\ \vdots \\ 0 \end{bmatrix}. \qquad (7)$$

In the following subsection, we will formulate the solution approach to the model problems in Eqs. 5 and 7.

2.2 Inverse Approach

We now aim to use the equivalent model problems in Eqs. 5 and 7 to formulate a least-squares (LS) minimization regime to solve the inverse problem. For illustration purposes, we begin by considering only one state, where $N = 1$ and the problem is unconstrained. In such a case, we aim to determine E_1 by minimizing the functional

$$\Psi^{\underline{1}}(E_1, F_1) = \left[||\Delta_1 - U_1(E_1, F_1)|| + ||\Gamma E_1|| \right] \qquad (8)$$

where $|| \cdot ||$ represents the L_2 norm, the superscript $\underline{1}$ denotes the degree of n (1, in this case), λ is the Tikhonov regularization parameter [66] which will be detailed later in this subsection, the regularization matrix is given by $\Gamma = \lambda \mathbb{I}$, and $\mathbb{I}$ is the identity matrix.

In general, however, we note that physically-realistic (non-complex) solutions are realized when $E_1 > 0$ – or more generally $E_n > 0$. Moreover, when prior information about the material is available, we may further constrain the problem such that the elasticity modulus is greater than some constant E_c known *a priori*. While still considering $N = 1$, we may rewrite the functional to be minimized as

$$\Psi^{\underline{1}}(E_1 > E_c, F_1) = \left[||\Delta_1 - U_1(E_1, F_1)|| + ||\Gamma E_1|| \right]. \qquad (9)$$

The extension of Eq. 9 for $N = 2$ is straightforward, and in the case of equal weighting of cost functions for each state n, is done by summation; i.e. for $N = 2$ we aim to minimize

$$\begin{aligned} \Psi^{\underline{N}}(E_n > E_c, F_n) &= \Psi^{\underline{1}}(E_1 > E_c, F_1) + \Psi^{\underline{2}}(E_2 > E_c, F_2) \\ &= \left[||\Delta_1 - U_1(E_1, F_1)|| + ||\Gamma E_1|| \right] \\ &\quad + \left[||\Delta_2 - U_2(E_2, F_2)|| + ||\Gamma E_2|| \right]. \end{aligned} \qquad (10)$$

In the general case, where N may take any positive integer, we aim to find the elastic modulus distributions $E_n{}^1$ that minimizes the following functional

$$\Psi^{\underline{N}}(E_n > E_c, F_n) = \sum_{n=1}^{N} \omega_n \left[||\Delta_n - U_n(E_n, F_n)|| + ||\Gamma E_n|| \right] \qquad (11)$$

where ω_n is the user-defined weight for each state. The inclusion of regularization in Eqs. 8 - 11 results from the ill-posed nature of the inverse problem, meaning that standard LS approaches may yield non-unique solutions. The form of regularization chosen here (L_2 regularization) is known to result in smooth solutions [67]. The primary advantage of this regularization technique is its simplicity: the smoothness of solutions is controlled by the magnitude of λ. For further information and discussion on more advanced regularization techniques incorporating structural prior information, we refer the reader to [68, 69]. We would like to note that (i) the constraints $E_n > E_c$ are handled using the interior point method and (ii) here, each state n is equally weighted during the minimization of Ψ such that $\sum_{n=1}^{N} \omega_n = 1$; however, biased weighting of each state n may also be employed in a straight-forward manner.

To compute the simulated displacement fields[2] U_n we employ the finite element method using

---

[1]We remark the E_n is a vector containing an inhomogeneous distribution of elastic modulii at each state n. In a discretized problem (such as herein), the size of E_n is equivalent to the number of elements in the discretization.

[2]Often, U_n is denoted the "forward model."

$$U_{n,j} = \sum_{i=1}^{q} K(E_n)_{ji}^{-1} F_{n,i} \qquad (12)$$

where q is the total number of unknown displacements, j, i denote the column and row locations, and K_{ji}^{-1} and F_i are often referred to as the compliance matrix and force vector, respectively [70, 71]. In this work, we use piece-wise linear triangular elements and neglect the effects of out-of-plane displacements (a plate in plane stress) in generating the stiffness matrix K_{ji}. We would like to comment that the structure of the well-known stiffness (or compliance) matrices within the FEM equations consisting of $F = KU$ or $U = K^{-1}F$ are positive definite (when properly constructed), which leads to unique solutions to the *forward problem* [71]. The ill posedness discussed herein refers to the inverse problem, wherein solutions (in this case E_n) to the inverse problem are highly sensitive to modeling errors and outlier data [68].

To solve the optimization problem we use a Gauss-Newton scheme equipped with a line-search function to compute the step size s_k in the parameterized (stacked) solution $\theta_k = \theta_{k-1} + s_k \bar{\theta}$ where θ_k is the current estimate and $\bar{\theta}$ is the LS update at iteration k. Within the parameterization, we define notation for the stacked vectors as follows: $\theta_k = [E_{1,k}, E_{2,k}, \ldots, E_{N,k}]^T$ and $\theta_{k-1} = [E_{1,k-1}, E_{2,k-1}, \ldots, E_{N,k-1}]^T$. For example, $E_{1,k}$ refers to $E_{n=1,k}$ or "$E_{n=1}$ at the kth iteration." Specifically, we define the stacked parameterizations

$$\theta_k = \begin{bmatrix} E_{1,k} \\ E_{2,k} \\ E_{3,k} \\ \vdots \\ E_{N,k} \end{bmatrix}, \; \theta_{k-1} = \begin{bmatrix} E_{1,k-1} \\ E_{2,k-1} \\ E_{3,k-1} \\ \vdots \\ E_{N,k-1} \end{bmatrix} \qquad (13)$$

and the stacked LS update

$$\bar{\theta} = \begin{bmatrix} (J_{E_{1,k-1}}^T J_{E_{1,k-1}} + \lambda \mathbb{I} + H_{E_1})^{-1} (J_{E_{1,k-1}}^T (\Delta_1 - U_1(E_{1,k-1})) - g_{E_1}) \\ (J_{E_{2,k-1}}^T J_{E_{2,k-1}} + \lambda \mathbb{I} + H_{E_2})^{-1} (J_{E_{2,k-1}}^T (\Delta_2 - U_2(E_{2,k-1})) - g_{E_2}) \\ (J_{E_{3,k-1}}^T J_{E_{3,k-1}} + \lambda \mathbb{I} + H_{E_3})^{-1} (J_{E_{3,k-1}}^T (\Delta_3 - U_3(E_{3,k-1})) - g_{E_3}) \\ \vdots \\ (J_{E_{N,k-1}}^T J_{E_{N,k-1}} + \lambda \mathbb{I} + H_{E_N})^{-1} (J_{E_{N,k-1}}^T (\Delta_N - U_N(E_{N,k-1})) - g_{E_N}) \end{bmatrix}$$
$$(14)$$

where H_{E_n} and g_{E_n} are the Hessian matrix and gradient vector, respectively, computed from the cubic polynomial barrier functions (for additional details regarding the implementation of barrier constraints in a LS

framework, like those used herein, we refer the reader to ([72, 73]), and $J_{E_n} = \frac{\partial U_n(E_n)}{\partial E_n}$ is the Jacobian. In this work, the Jacobian at each state $J_{E_n} = \frac{\partial U_n(E_n)}{\partial E_n}$ is computed at each iteration using the perturbation method with central differencing, where the entries are calculated using

$$J_{E_n,ij} = \frac{U_n(E_{n,k-1} + p) - U_n(E_{n,k-1} - p)}{2p} \qquad (15)$$

where the perturbation p is computed as a function of the machine precision ε using $p = \sqrt[3]{\frac{\varepsilon}{2}}$ following [74].

As with many optimization problems, some stopping criteria φ must be defined; in this work we found $\varphi = (\Psi_k - \Psi_{k-5})/\Psi_{k-5} \leq 10^{-3}$ to be satisfactory. In particular, the use of Ψ_{k-5} was selected to help ensure that the cost function has reached a stable minimum in the case there are oscillations at later iterations. Lastly, the final optimized distribution of the elasticity modulus E_Ψ must be computed. To be consistent with the equal weighting employed in the minimization of Ψ in Eq. 11, we simply compute E_Ψ using the mean value for each discretized element in the solution vector θ.

Remark: We would like to mention that the proposed method is also versatile to optimize other structural and material parameters. For example, one may modify Eqs. 11, 12, 13, 14, and 15 in a straight-forward manner to solve the optimization problem with respect to the Poisson ratio ν, shear modulus G, or plate thickness t. In cases where multiple parameters, for example E and t, are optimized simultaneously, one may incorporate a parameterization regime such as the one proposed in [75, 76].

3 Numerical examples

The following numerical examples are designed to test the proposed approach and demonstrate optimized distributions of the elastic modulus E_Ψ in structural elements with $N = 2$. In the first two examples, we examine the rectangular beam-columns. For the first two examples, (i) the design displacement targets Δ_1 and Δ_2 are selected as simple functions in the x, y coordinate plane and (ii) the constraint E_c was selected such that the displacement fields were small during the initial iterations. In the third example, we study the effect of mesh size the constraint E_c on the inverse solutions for an irregular geometry; we also consider the numerical behavior during minimization of the cost function. In

the examples, we neglect out of plane deformations, i.e. the structural elements are in plane stress. For simplicity, we use dimensionless units for the deformations, forces, elastic coefficients, and coordinate system.

In solving each problem, we select $\lambda = 10^{-3}$ and make no further attempt to optimize the regularization parameter during iterations. Lastly, all problems were solved using a `MATLAB` implementation of the algorithm described in section 2 and the choice of the domain meshing was selected based on available computational resources.

3.1 Example 1: non-slender beam column

In this example, we consider a cantilevered beam clamped at $y = 0$ with two design displacement targets, a homogeneous Poisson ratio $\nu = 0.35$, and plate thickness $t = 0.2$. The first design displacement target takes the form of a cubic polynomial where the mesh points of the unloaded beam are displaced by the following function $\Delta_1(x,y) = [0.005y^3 - 0.07y^2 + 0.2y, -]$, where the y coordinate refers to the vertical coordinates along the beam (note that the y-coordinates were intentionally not translated). The second target is given by a pure axial translation of the form $\Delta_2(x,y) = [-, 0.01y]$. The design displacement targets and loading for each criterion are shown in Fig. 1 plotted atop the displaced triangulation consisting of 800 elements. Moreover, in determining E_Ψ, we utilized the constraint $E_c = 30$.

(a) **(b)**
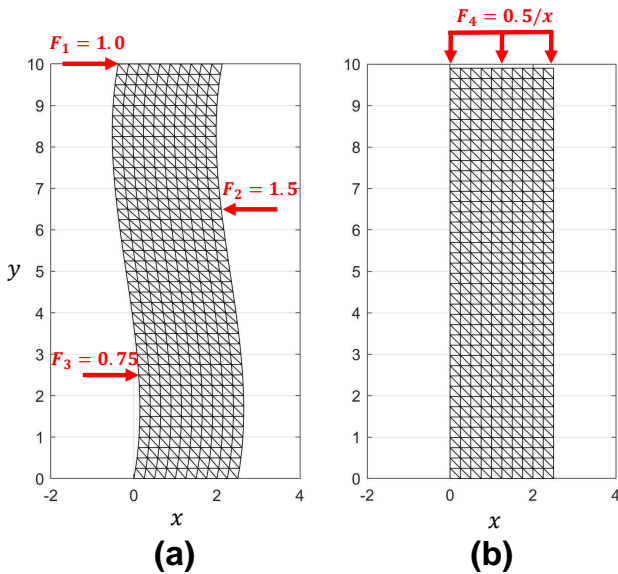
Fig. 1. Example 1: Schematic detailing the external forces and structural elements deformed by the design displacement targets (a) Δ_1, a cubic polynomial translating the x grid coordinates and (b) Δ_2, a pure axial translation along the y-axis.

The solution for this example is shown in Fig. 2, with optimized E_Ψ plotted atop displaced configurations generated from simulated displacement fields $U_1 = U_1(E_\Psi, F_1, F_2, F_3)$ and $U_2 = U_2(E_\Psi, F_4)$, which correspond to displacement targets Δ_1 and Δ_2, respectively. Results shown in Fig. 2 show a highly inhomogenous distribution of the elasticity modulus. This is a satisfactory and expected result, given (a) the non-physical nature of Δ_1, where the y-components of the field were not translated as would be observed in physically-realistic bending case (i.e. Δ_1 did not consider rotations) and (b) the applied forces are not congruent with the displacement fields prescribed in Δ_1 and Δ_2. It is therefore apparent why areas of the beam have been stiffened and softened to compensate for discrepancies between the forces and prescribed displacement fields.

(a) **(b)**
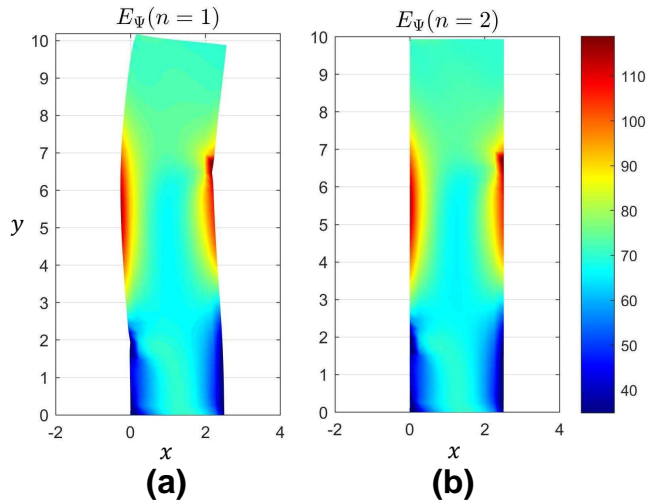
Fig. 2. Optimized distribution of E_Ψ for Example 1, (a) E_Ψ plotted atop U_1 and (b) E_Ψ plotted atop U_2. The right-hand side color bar indicates the magnitude of inhomogeneous E_Ψ in each image.

It is interesting to note that near the location of the largest applied point force, F_2, there is an obvious local increase in E_Ψ. This results from local data mismatch between the smooth field Δ_1 and the locally-perturbed field U_1. The local increase in stiffness near F_2 is therefore consistent with this realization. Moreover, upon comparing Figs. 1 and 2 we observe that U_1 and Δ_1 are not a perfect match - despite meeting the minimization criterion φ. On the other hand, we observe that U_2 and Δ_2 compare more favorably. Central reasons for these observations are (i) the previously noted unrealistic nature of Δ_1 (in contrast to Δ_2, which is a realistic description of an axial displacement field), (ii)

the ill-posed nature of the inverse problem, (iii) the increased non-uniqueness in stacked parameterizations of inverse problems (also noted in [75,76], (iv) the use the L_2 regularization, an uninformative prior model, (v) the regularization parameter λ was not optimized at each iteration, and (vi) the effects of weighting the solution E_Ψ.

3.2 Example 2: slender beam column

In this example, we consider a slender beam with $t = 0.1$ and $\nu = 0.35$. The beam is clamped at $y = 0$ and pinned at the coordinates $(x,y) = [1,10]$ without the presence of axial loads. The first displacement target is quadratic and has the form $\Delta_1(x,y) = [-0.015y^2 + 0.15y, -]$. The second target is a cubic function given by $\Delta_1(x,y) = [0.005y^3 - 0.08y^2 + 0.25y, -]$. No translation in the y-direction is prescribed. The target displacement fields and loading for each criterion are shown in Fig. 3 plotted atop the displaced triangulation consisting of 980 elements. The constraint was chosen as $E_c = 100$.

(a)   **(b)**
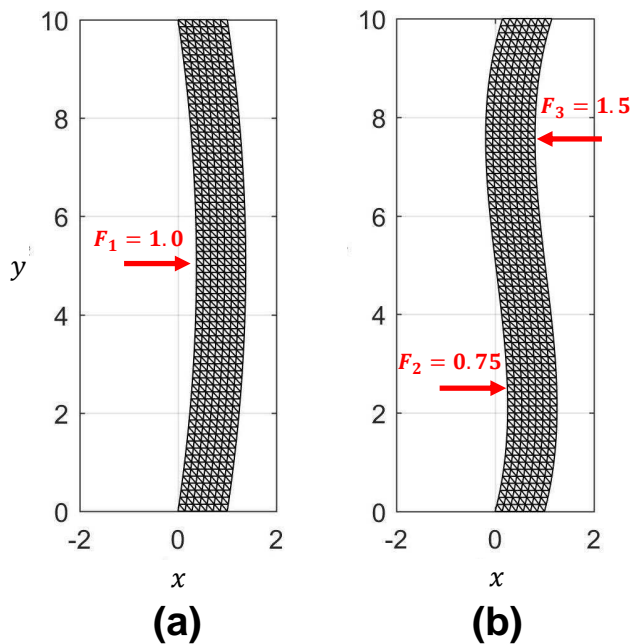
Fig. 3. Example 2: Schematic detailing the external forces and structural elements deformed by the design displacement targets (a) Δ_1, a quadratic polynomial translating the x grid coordinates and (b) Δ_2 a cubic polynomial translating the x grid coordinates.

The solution for this example is shown in Fig. 4, with optimized E_Ψ plotted atop displaced configurations generated from simulated displacement fields

$U_1 = U_1(E_\Psi, F_1)$ and $U_2 = U_2(E_\Psi, F_2, F_3)$, which correspond to displacement targets Δ_1 and Δ_2, respectively. We again observe a highly inhomogenous distribution of the solution E_Ψ, especially in the areas of high curvature. As in Example 1, the local stiffening and softening observed in E_Ψ is largely affected by the local discrepancies between the simulated displacement fields and target displacement fields. Of note, significant stiffening is observed near the pinned connection at $(x,y) = [1,10]$ and the negative moment region at the clamped base as the inverse model is compensating for localized effects resulting from high deformations gradients.

(a)   **(b)**
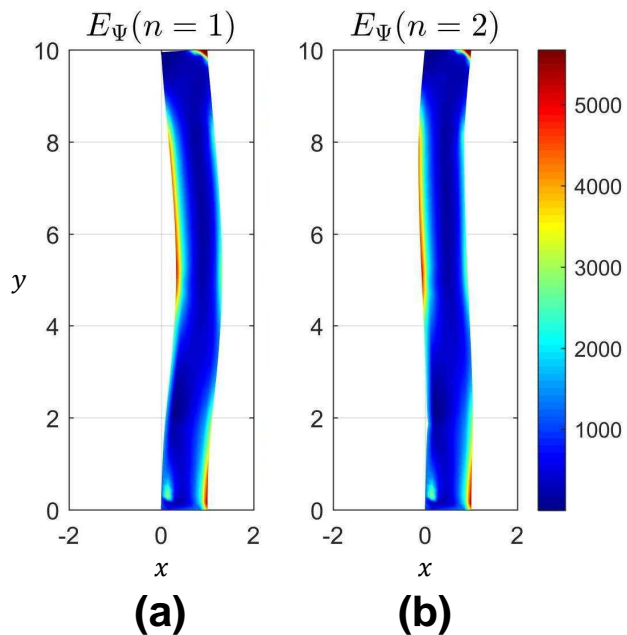
Fig. 4. Optimized distribution of E_Ψ for Example 2, (a) E_Ψ plotted atop U_1 and (b) E_Ψ plotted atop U_2. The right-hand side color bar indicates the magnitude of inhomogeneous E_Ψ in each image.

Relative to the beam in Example 1, the beam in this example is markedly more slender. This led to a significant differences in the distribution of the elastic modulus in the solution. Upon observation of Fig. 4, it is apparent that the variability of E_Ψ is much higher than the variability observed in Fig 2. This is most plausibly due to the lower shear stresses occurring in the more slender beam. In the case of slender beams, differences in the simulated and target displacement fields are most significantly compensated by changes in the bending stiffness near the top and bottom of the beam cross sections. On the other hand, solutions for deeper beams are more dependent on effects near the neutral

axis of the member due to shear effects. Bearing this realization in mind, is important to note that, while differences in the aspect ratio of the member do have important implications on the global distribution of E_Ψ, the effects of external loads and boundary conditions also have significant local implications on E_Ψ.

3.3 Example 3: Irregular member considering the effects of mesh size and constraints

In the final example, we consider an irregular member with $t = 0.25$ and $\nu = 0.35$. The member is clamped at $y = 0$. The first target displacement is of the form $\Delta_1 = [0.005y^2, -0.005x^2]$ and the second target displacement is a linear translation of the form $\Delta_2 = [0.02y, -]$. Two discretizations are considered, the first mesh, denoted the coarse mesh, consists of 67 triangular elements. The second discretization considered has 247 elements, and is denoted the refined mesh. The target displacement fields and loading for each criterion are shown in Fig. 5 plotted atop the displaced triangulations.

The solutions for this example are shown in Fig. 6, with optimized E_Ψ plotted atop displaced configurations generated from simulated displacement fields $U_1 = U_1(E_\Psi, F_1)$ and $U_2 = U_2(E_\Psi, F_2)$, which correspond to displacement targets Δ_1 and Δ_2, respectively. We observe that, in general, the obtained solutions have similar distributions of E_Ψ. Indeed, we clearly observe, in all images, that the column portion of the member is significantly more stiffened relative to the horizontal member due to the bending moments resulting from F_2. On the other hand, since the horizontal member is in a state of axial tension in the second state, the optimized stiffness for the horizontal component is considerably lower than the vertical component. This is therefore an expected result.

In comparing the results obtained using different discretizations, we note two primary differences in the solutions: the distribution of the elastic modulus at the base of the column and near the location of F_1. In solutions obtained using the coarse mesh, there is significant stiffening near the base and nodal force. This observation results from two realizations, (a) that coarser meshes are known to decrease model accuracy during stiffness integration, in many cases increasing stiffness [70] and (b) coarser meshes decrease the degrees of freedom for solutions (E_Ψ) in the inverse problem. Based on (a), it is no surprise that the increased element and global stiffness resulting from coarse forward modeling is reflected in the inverse solutions. With regards to point (b), it is apparent that by reducing the degrees

(a)

(b)
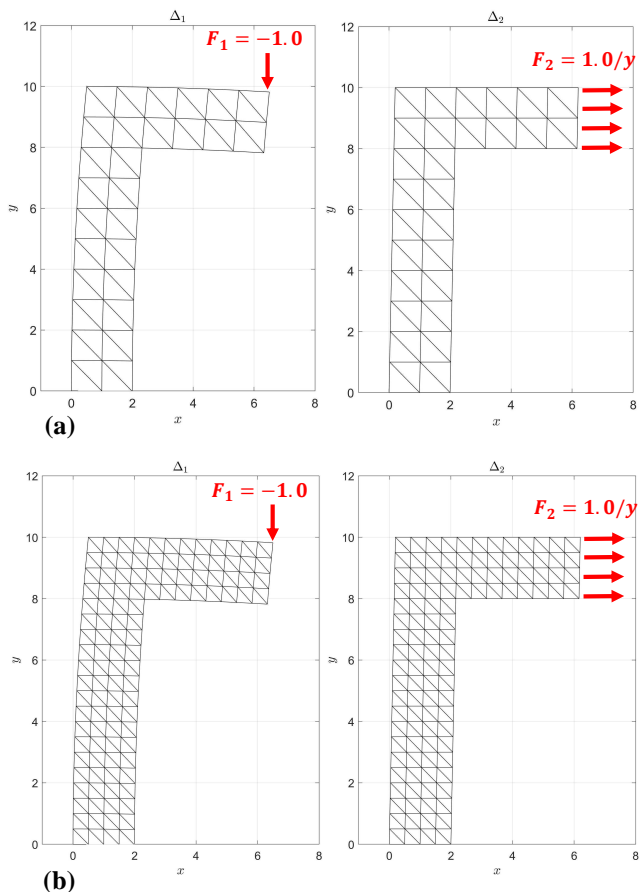
Fig. 5. Example 3: Schematic detailing the external forces and structural elements deformed by the design displacement targets Δ_1 and Δ_2 for (a) a coarse triangular discretization and (b) a refined triangular discretization.

of freedom in E_Ψ, the coarse solutions are smoother since small localized fluctuations of E_Ψ are not possible. Solutions obtained with the fine mesh, on the other hand, do have small fluctuations which may be viewed as artifacts resulting from the non-uniqueness of the inverse problem and the non-optimized regularization parameter [68].

For results reported in this section, the effect of the lower constraint E_c on the optimized solutions of E_Ψ is more subtle than the effect of discretization. The effect of E_c was similar for solutions obtained using coarse and fine meshes: the results were smoother for $E_c > 50$ than for $E_c > 0$. The reason for this is that the available solutions[3] of E_Ψ are more restricted and closer to the average optimal values of E_Ψ.

Of particular interest in optimization problems is

---

[3] In a rough sense, the degrees of freedom or possibilities for the elasticity modulus are decreased by constraining the optimization problem. We would like to remark, however this is not necessarily equivalent to the added spatial degrees of freedom provided by mesh refinement.

(a)

(b)

(c)

(d)
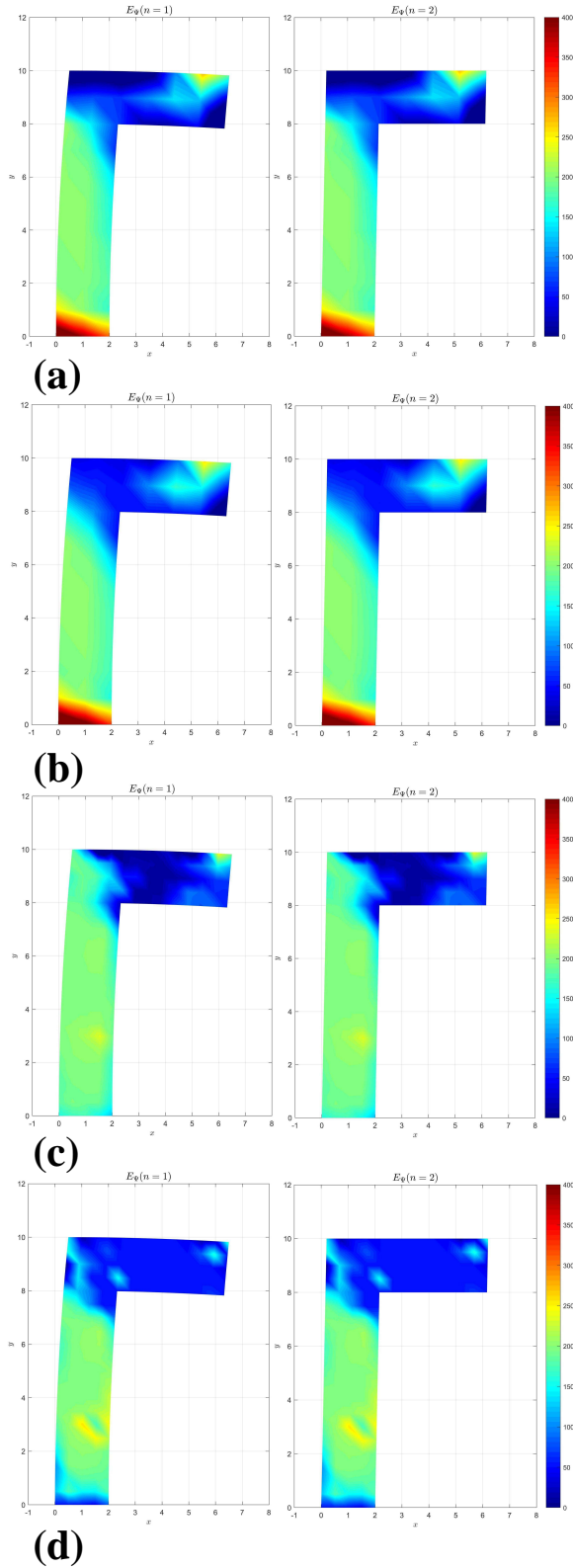
Fig. 6. Optimized distributions of E_Ψ for Example 3 for (a) the coarse mesh with $E_c > 0$, (b) the coarse mesh with $E_c > 50$, (c) the refined mesh with $E_c > 0$, and (d) the refined mesh with $E_c > 50$.

the minimization rate of the cost function, which sheds light on the computational efficiency of the regime. Here, we compare the minimization rate for both discretizations and consider the effect E_c has on the final solution once the stopping criteria is reached. The minimization curves for the cost function Ψ as a function of the iteration number k are shown in Fig.7.
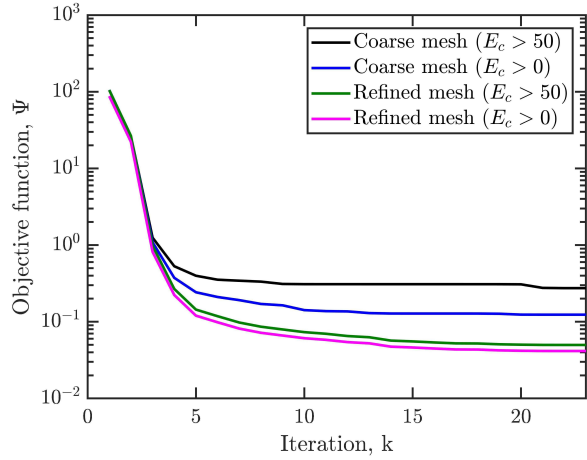
Fig. 7. Minimization curves for the cost function Ψ as a function of the iteration number k considering the lower constraint E_c and the discretization.

The minimization curves shown in Fig 7 support the earlier statements regarding the behavior of the optimization problem with respect to the effects of the constraint E_c and the mesh refinement; this will be discussed in the following. While the minimization rates of Ψ for both the discretizations were similar, the refined meshes reached a lower minimum for both $E_c > 0$ and $E_c > 50$. Moreover, for both the coarse and fine meshes, $E_c > 0$ resulted in lower minimum values of Ψ. These results indicate that by increasing the degrees of freedom available for the inverse solution (via decreasing E_c and increasing the spatial degrees of freedom), the optimized solution for E_Ψ reached a more globally optimized solution.

3.4 Discussion

In this section, we examined optimized solutions of the elastic modulus E_Ψ for 2D rectangular beams and an irregularly shaped beam-column considering different loading, boundary conditions, target displacement fields, and aspect ratios using the proposed regime. In the analysis of the irregularly-shaped beam column, the effects of the lower constraint E_c and discretization were investigated. As a whole, the proposed opti-

mization regime and the solutions obtained were determined to be physically and intuitively consistent. We noted multiple factors contributing the inhomgeneity, variability, and distribution of the optimized solutions. Some of the important contributors in solution of E_Ψ included (in no specific order):

1. Global effects related to the geometry of structural elements.
2. Local effects resulting from external forces and imposed boundary conditions.
3. The (possibly) non-physical nature of prescribed displacement fields Δ_n.
4. Effects from not optimizing the regularization parameter λ.
5. Effects from weighting E_Ψ.
6. Local and global effects due to mesh size.
7. Global effects related to the lower constraint E_c.

It is tempting to draw general conclusions as to which variable contributes most to the optimized solution E_Ψ or to which parameter the inverse problem is most sensitive. However, when we consider the coupled non-uniqueness of the inverse problem, number of structural states stacked, complexity of boundary/loading conditions, and prior information; we may surmise that solutions of E_Ψ are highly application specific.

We would like to remark that this article has focused primarily on the numerical regimes, minimization techniques, and interpretation of the results in idealized cases. However, it should be noted that current manufacturing techniques used to generate spatial inhomogeneity in elastic properties such as the Young's modulus or Poisson's ratio have limitations. In such cases, we may expect manufacturing processes to have band-limited ranges and constraints. These constraints may, indeed, be used within the constrained optimization scheme by incorporating upper and lower barrier functions at the extremes of the manufacturing bounds. As results of this article have shown, the use of constraints decreases the degrees of freedom and may result in a less optimized solution relative to a problem contrained to be only physically realistic (e.g. $E > 0$).

4   Conclusions

In this article, we proposed a constrained least-squares approach for computationally optimizing the distribution of the elastic modulus for N states. Each state was defined by different loading conditions and target displacement fields that may be prescribed by the designer. A numerical study was conducted to test the approach, where 2D structural elements with different aspect ratios, geometries, loading/boundary conditions, and target displacement fields were analyzed. The approach was tested for $N = 2$, where results were demonstrated to be physically-realistic and intuitively consistent. It was noted that optimized distributions of the elastic modulus were affected by important factors, such as the structural geometry, prior information, solution weighting, physically-realistic nature of the target displacement fields, imposed constraints, discretization, and overall non-uniqueness of the inverse problem.

References

[1] Zegard, T., and Paulino, G. H., 2016. "Bridging topology optimization and additive manufacturing". *Structural and Multidisciplinary Optimization,* **53**(1), pp. 175–192.

[2] Deaton, J. D., and Grandhi, R. V., 2014. "A survey of structural and multidisciplinary continuum topology optimization: post 2000". *Structural and Multidisciplinary Optimization,* **49**(1), pp. 1–38.

[3] Bendsoe, M. P., and Sigmund, O., 2013. *Topology optimization: theory, methods, and applications.* Springer Science & Business Media.

[4] Sigmund, O., 2001. "A 99 line topology optimization code written in matlab". *Structural and Multidisciplinary Optimization,* **21**(2), pp. 120–127.

[5] Zhou, M., and Rozvany, G., 1991. "The coc algorithm, part ii: topological, geometrical and generalized shape optimization". *Computer Methods in Applied Mechanics and Engineering,* **89**(1-3), pp. 309–336.

[6] Bendsøe, M. P., and Kikuchi, N., 1988. "Generating optimal topologies in structural design using a homogenization method". *Computer Methods in Applied Mechanics and Engineering,* **71**(2), pp. 197–224.

[7] Maute, K., Tkachuk, A., Wu, J., Qi, H. J., Ding, Z., and Dunn, M. L., 2015. "Level set topology

optimization of printed active composites". *Journal of Mechanical Design,* **137**(11), p. 111402.

[8] van Dijk, N. P., Maute, K., Langelaar, M., and Van Keulen, F., 2013. "Level-set methods for structural topology optimization: a review". *Structural and Multidisciplinary Optimization,* **48**(3), pp. 437–472.

[9] Yamada, T., Izui, K., Nishiwaki, S., and Takezawa, A., 2010. "A topology optimization method based on the level set method incorporating a fictitious interface energy". *Computer Methods in Applied Mechanics and Engineering,* **199**(45-48), pp. 2876–2891.

[10] Allaire, G., Jouve, F., and Toader, A.-M., 2004. "Structural optimization using sensitivity analysis and a level-set method". *Journal of Computational Physics,* **194**(1), pp. 363–393.

[11] Wang, M. Y., Wang, X., and Guo, D., 2003. "A level set method for structural topology optimization". *Computer Methods in Applied Mechanics and Engineering,* **192**(1-2), pp. 227–246.

[12] Blank, L., Garcke, H., Sarbu, L., Srisupattarawanit, T., Styles, V., and Voigt, A., 2012. "Phase-field approaches to structural topology optimization". In *Constrained Optimization and Optimal Control for Partial Differential Equations.* Springer, pp. 245–256.

[13] Dedè, L., Borden, M. J., and Hughes, T. J., 2012. "Isogeometric analysis for topology optimization with a phase field model". *Archives of Computational Methods in Engineering,* **19**(3), pp. 427–465.

[14] Takezawa, A., Nishiwaki, S., and Kitamura, M., 2010. "Shape and topology optimization based on the phase field method and sensitivity analysis". *Journal of Computational Physics,* **229**(7), pp. 2697–2718.

[15] Czarnecki, S., and Lewiński, T., 2017. "On material design by the optimal choice of young's modulus distribution". *International Journal of Solids and Structures,* **110**, pp. 315–331.

[16] Ben-Tal, A., Kocvara, M., Nemirovski, A., and Zowe, J., 1999. "Free material design via semidefinite programming: The multiload case with contact conditions". *SIAM Journal on Optimization,* **9**(4), pp. 813–832.

[17] Zuo, W., and Saitou, K., 2017. "Multi-material topology optimization using ordered simp interpolation". *Structural and Multidisciplinary Optimization,* **55**(2), pp. 477–491.

[18] Sivapuram, R., Dunning, P. D., and Kim, H. A.,

2016. "Simultaneous material and structural optimization by multiscale topology optimization". *Structural and Multidisciplinary Optimization,* **54**(5), pp. 1267–1281.

[19] Tavakoli, R., 2014. "Multimaterial topology optimization by volume constrained allen–cahn system and regularized projected steepest descent method". *Computer Methods in Applied Mechanics and Engineering,* **276**, pp. 534–565.

[20] Guo, X., Zhang, W., and Zhong, W., 2014. "Doing topology optimization explicitly and geometrically—a new moving morphable components based framework". *Journal of Applied Mechanics,* **81**(8), p. 081009.

[21] Ramani, A., 2011. "Multi-material topology optimization with strength constraints". *Structural and Multidisciplinary Optimization,* **43**(5), pp. 597–615.

[22] Cramer, A. D., Challis, V. J., and Roberts, A. P., 2016. "Microstructure interpolation for macroscopic design". *Structural and Multidisciplinary Optimization,* **53**(3), pp. 489–500.

[23] Bendsoe, M. P., Guedes, J., Haber, R. B., Pedersen, P., and Taylor, J., 1994. "An analytical model to predict optimal material properties in the context of optimal structural design". *Journal of Applied Mechanics,* **61**(4), pp. 930–937.

[24] Ringertz, U., 1993. "On finding the optimal distribution of material properties". *Structural Optimization,* **5**(4), pp. 265–267.

[25] Maar, B., and Schulz, V., 2000. "Interior point multigrid methods for topology optimization". *Structural and Multidisciplinary Optimization,* **19**(3), pp. 214–224.

[26] Kočvara, M., Zibulevsky, M., and Zowe, J., 1998. "Mechanical design problems with unilateral contact". *ESAIM: Mathematical Modelling and Numerical Analysis,* **32**(3), pp. 255–281.

[27] Zowe, J., Kočvara, M., and Bendsøe, M. P., 1997. "Free material optimization via mathematical programming". *Mathematical Programming,* **79**(1-3), pp. 445–466.

[28] Jarre, F., Kočvara, M., and Zowe, J., 1996. *Interior point methods for mechanical design problems.* Universität Erlangen-Nürnberg. Institut für Angewandte Mathematik.

[29] Allaire, G., Jouve, F., and Maillot, H., 2004. "Topology optimization for minimum stress design with the homogenization method". *Structural and Multidisciplinary Optimization,* **28**(2-3), pp. 87–98.

[30] Pereira, J., Fancello, E., and Barcellos, C., 2004. "Topology optimization of continuum structures with material failure constraints". *Structural and Multidisciplinary Optimization,* **26**(1-2), pp. 50–66.

[31] Kočvara, M., and Stingl, M., 2007. "Free material optimization for stress constraints". *Structural and Multidisciplinary Optimization,* **33**(4-5), pp. 323–335.

[32] Kočvara, M., and Stingl, M., 2007. "On the solution of large-scale sdp problems by the modified barrier method using iterative solvers". *Mathematical Programming,* **109**(2-3), pp. 413–444.

[33] Stingl, M., 2006. *On the solution of nonlinear semidefinite programs by augmented Lagrangian methods*. Shaker Aachen.

[34] Deng, S., and Suresh, K., 2017. "Stress constrained thermo-elastic topology optimization with varying temperature fields via augmented topological sensitivity based level-set". *Structural and Multidisciplinary Optimization,* **56**(6), pp. 1413–1427.

[35] Haslinger, J., Kočvara, M., Leugering, G., and Stingl, M., 2010. "Multidisciplinary free material optimization". *SIAM Journal on Applied Mathematics,* **70**(7), pp. 2709–2728.

[36] Picelli, R., Townsend, S., Brampton, C., Norato, J., and Kim, H., 2018. "Stress-based shape and topology optimization with the level set method". *Computer Methods in Applied Mechanics and Engineering,* **329**, pp. 1–23.

[37] Zhang, S., Gain, A. L., and Norato, J. A., 2017. "Stress-based topology optimization with discrete geometric components". *Computer Methods in Applied Mechanics and Engineering,* **325**, pp. 1–21.

[38] Le, C., Norato, J., Bruns, T., Ha, C., and Tortorelli, D., 2010. "Stress-based topology optimization for continua". *Structural and Multidisciplinary Optimization,* **41**(4), pp. 605–620.

[39] Czarnecki, S., and Wawruch, P., 2015. "The emergence of auxetic material as a result of optimal isotropic design". *Physica Status Solidi (b),* **252**(7), pp. 1620–1630.

[40] Czubacki, R., and Lewiński, T., 2015. "Topology optimization of spatial continuum structures made of non-homogeneous material of cubic symmetry". *Journal of Mechanics of Materials and structures,* **10**(4), pp. 519–535.

[41] Brańka, A., Heyes, D., and Wojciechowski, K., 2009. "Auxeticity of cubic materials". *Physica Status Solidi (b),* **246**(9), pp. 2063–2071.

[42] Brańka, A., and Wojciechowski, K., 2008. "Auxeticity of cubic materials: The role of repulsive core interaction". *Journal of Non-Crystalline Solids,* **354**(35-39), pp. 4143–4145.

[43] Coelho, P. G., Cardoso, J. B., Fernandes, P. R., and Rodrigues, H. C., 2011. "Parallel computing techniques applied to the simultaneous design of structure and material". *Advances in Engineering Software,* **42**(5), pp. 219–227.

[44] Liu, L., Yan, J., and Cheng, G., 2008. "Optimum structure with homogeneous optimum truss-like material". *Computers & Structures,* **86**(13-14), pp. 1417–1425.

[45] Cheng, G., Liu, L., and Yan, J., 2006. "Optimum structure with homogeneous optimum truss-like material". In III European Conference on Computational Mechanics, Springer, pp. 481–481.

[46] Gosselin, C., Duballet, R., Roux, P., Gaudillière, N., Dirrenberger, J., and Morel, P., 2016. "Large-scale 3d printing of ultra-high performance concrete–a new processing route for architects and builders". *Materials & Design,* **100**, pp. 102–109.

[47] Feng, P., Meng, X., Chen, J.-F., and Ye, L., 2015. "Mechanical properties of structures 3d printed with cementitious powders". *Construction and Building Materials,* **93**, pp. 486–497.

[48] Radman, A., Huang, X., and Xie, Y., 2013. "Topology optimization of functionally graded cellular materials". *Journal of Materials Science,* **48**(4), pp. 1503–1510.

[49] Liu, W., and DuPont, J., 2003. "Fabrication of functionally graded tic/ti composites by laser engineered net shaping". *Scripta Materialia,* **48**(9), pp. 1337–1342.

[50] Wang, X., Xu, S., Zhou, S., Xu, W., Leary, M., Choong, P., Qian, M., Brandt, M., and Xie, Y. M., 2016. "Topological design and additive manufacturing of porous metals for bone scaffolds and orthopaedic implants: a review". *Biomaterials,* **83**, pp. 127–141.

[51] Hollister, S. J., 2005. "Porous scaffold design for tissue engineering". *Nature materials,* **4**(7), p. 518.

[52] Evgrafov, A., 2005. "The limits of porous materials in the topology optimization of stokes flows". *Applied Mathematics and Optimization,* **52**(3), pp. 263–277.

[53] Yaji, K., Yamada, T., Kubo, S., Izui, K., and Nishiwaki, S., 2015. "A topology optimization method

for a coupled thermal–fluid problem using level set boundary expressions". *International Journal of Heat and Mass Transfer,* **81**, pp. 878–888.

[54] Garcke, H., Hecht, C., Hinze, M., and Kahle, C., 2015. "Numerical approximation of phase field based shape and topology optimization for fluids". *SIAM Journal on Scientific Computing,* **37**(4), pp. A1846–A1871.

[55] Guest, J. K., and Prévost, J. H., 2006. "Topology optimization of creeping fluid flows using a darcy–stokes finite element". *International Journal for Numerical Methods in Engineering,* **66**(3), pp. 461–484.

[56] Borrvall, T., and Petersson, J., 2003. "Topology optimization of fluids in stokes flow". *International journal for numerical methods in fluids,* **41**(1), pp. 77–107.

[57] Pizzolato, A., Sharma, A., Maute, K., Sciacovelli, A., and Verda, V., 2017. "Topology optimization for heat transfer enhancement in latent heat thermal energy storage". *International Journal of Heat and Mass Transfer,* **113**, pp. 875–888.

[58] Jing, G., Isakari, H., Matsumoto, T., Yamada, T., and Takahashi, T., 2015. "Level set-based topology optimization for 2d heat conduction problems using bem with objective function defined on design-dependent boundary with heat transfer boundary condition". *Engineering Analysis with Boundary Elements,* **61**, pp. 61–70.

[59] Gersborg-Hansen, A., Bendsøe, M. P., and Sigmund, O., 2006. "Topology optimization of heat conduction problems using the finite volume method". *Structural and multidisciplinary optimization,* **31**(4), pp. 251–259.

[60] Deng, S., and Suresh, K., 2017. "Topology optimization under thermo-elastic buckling". *Structural and Multidisciplinary Optimization,* **55**(5), pp. 1759–1772.

[61] Deng, S., and Suresh, K., 2016. "Multiconstrained 3d topology optimization via augmented topological level-set". *Computers & Structures,* **170**, pp. 1–12.

[62] Deng, S., and Suresh, K., 2015. "Multiconstrained topology optimization via the topological sensitivity". *Structural and Multidisciplinary Optimization,* **51**(5), pp. 987–1001.

[63] Sokół, T., and Rozvany, G., 2013. "On the adaptive ground structure approach for multi-load truss topology optimization". In 10th World Congress on Structural and Multidisciplinary Optimization, pp. 19–24.

[64] Alvarez, F., and Carrasco, M., 2005. "Minimization of the expected compliance as an alternative approach to multiload truss optimization". *Structural and Multidisciplinary optimization,* **29**(6), pp. 470–476.

[65] Guedes, J. M., Rodrigues, H. C., and Bendsøe, M. P., 2003. "A material optimization model to approximate energy bounds for cellular materials under multiload conditions". *Structural and Multidisciplinary Pptimization,* **25**(5-6), pp. 446–452.

[66] Tikhonov, A. N., and Glasko, V. B., 1965. "Use of the regularization method in non-linear problems". *USSR Computational Mathematics and Mathematical Physics,* **5**(3), pp. 93–107.

[67] Vauhkonen, M., Vadasz, D., Karjalainen, P. A., Somersalo, E., and Kaipio, J. P., 1998. "Tikhonov regularization and prior information in electrical impedance tomography". *IEEE Transactions on Medical Imaging,* **17**(2), pp. 285–293.

[68] Mueller, J. L., and Siltanen, S., 2012. *Linear and nonlinear inverse problems with practical applications.* SIAM.

[69] Kaipio, J., and Somersalo, E., 2006. *Statistical and computational inverse problems,* Vol. 160. Springer Science & Business Media.

[70] Surana, K. S., and Reddy, J., 2016. *The Finite Element Method for Boundary Value Problems: Mathematics and Computations.* CRC Press.

[71] Oberai, A. A., Gokhale, N. H., Doyley, M. M., and Bamber, J. C., 2004. "Evaluation of the adjoint equation based algorithm for elasticity imaging". *Physics in Medicine and Biology,* **49**(13), p. 2955.

[72] Kim, S.-J., Koh, K., Lustig, M., Boyd, S., and Gorinevsky, D., 2007. "An interior-point method for large-scale l1-regularized least squares". *IEEE journal of selected topics in signal processing,* **1**(4), pp. 606–617.

[73] Vauhkonen, M., 1997. "Electrical impedance tomography and prior information".

[74] An, H.-B., Wen, J., and Feng, T., 2011. "On finite difference approximation of a matrix-vector product in the jacobian-free newton–krylov method". *Journal of Computational and Applied Mathematics,* **236**(6), pp. 1399 – 1409.

[75] Smyl, D., Bossuyt, S., and Liu, D., Submitted, 2018. "Stacked elasticity imaging approach for visualizing defects in the presence of background inhomogeneity". *Journal of Engineering Mechanics.*

[76] Liu, D., Kolehmainen, V., Siltanen, S., Laukkanen, A., and Seppänen, A., 2015. "Estimation of

conductivity changes in a region of interest with electrical impedance tomography". *Inverse Problems and Imaging,* **9(1)**, pp. 211–229.